# INVESTIGATION OF THERMAL BEHAVIOR AND MICROSTRUCTURE OF CARBON ADDED NiTi SHAPE MEMORY ALLOYS

*Ercan Ercan*[*1] iD

[1]*Bitlis Eren Üniversitesi, Fen Edebiyat Fakültesi, Fizik Bölümü. Bitlis/Türkiye*

## Abstract

*Original scientific paper*

This study aims to examine the thermal and microstructural properties of NiTiC1 and NiTiC2 shape memory alloys (SMAs) produced by arc-melting method. It was observed that additive C did not alter the phase transformation order which remained as one-step ($B2 \leftrightarrow B19'$). Additionally, the effect of C addition on thermal properties of the Ni-riched NiTi alloy(s), including temperature hysteresis, enthalpy, entropy, and Gibbs free energies were also determined. An increase in the amount of C noticeably reduced the detectable grain size and thus decreased the elastic energy of the alloy. In DSC analysis, the presence of martensitic phases in the alloys was determined below the room temperature. The presence of B2 austenite, $Ni_4Ti_3$ precipitate, and TiC phases were detected in XRD analyses, which were supported by SEM-EDX results. Grain boundaries were clearly observed and precipitates were found to be homogeneously distributed.

*Keywords:* Shape memory alloy, NiTiC, elastic energy, gibbs free energy, grain size.

## 1 Introduction

Smart materials are becoming increasingly important as technology develops, e.g., they are used as sensors, actuators, and fasteners in some fields such as space, industry, and medicine [1-3]. The important role that shape memory alloys (SMAs), which are a class of smart materials, play is due to the shape memory effect (SME) and pseudo-elasticity [4, 5]. In terms of low-temperature range martensitic phase transformation, NiTi alloys constitute the most important group of alloys [2, 6]. Some methods can be used to adjust the required transformation temperatures depending on the applications of NiTi SMAs [7, 8]. For example, changing the element ratios of the alloy, adding different elements, changing the homogenization temperature, and quenching conditions [9, 10].

Controlling the phase transformation of Ni-rich NiTi SMAs at room temperature is necessary for some of the technologies operating in this range [11-13]. However, the presence of metastable intermediate phases ($Ni_4Ti_3$, $Ni_3Ti_2$) that affect the transformation temperatures in Ni-rich NiTi alloys are undesirable [11, 14]. Researchers are attempting to alloy with a third element to minimize these undesirable phases in Ni-rich NiTi alloys system in a way that does not have a significant effect on phase transformation temperatures [15-20]. However, studies on Ni-rich NiTiC alloys at the desired transformation temperature and structure are limited.

The variation of the transformation temperatures strongly depends on the elemental concentration of the alloys [4, 6]. The change of elemental concentration causes changes in transformation temperatures as well as other thermodynamic parameters such as enthalpy, entropy, and Gibbs free energy. The most widely used thermal analysis system to examine these parameters is Differential Scanning Calorimetry (DSC) instrument [21]. As a matter of fact, transformation temperatures and enthalpy can be easily calculated with the help of the heating/cooling curves obtained by the DSC measurements. The Gibbs free energy, entropy, and enthalpy values of NiTiC alloys have been investigated previously [15]. However, appropriate information such as elastic energy and grain size is not found in the literature for NiTiC alloys.

In this study, it is aimed to determine transformation temperatures and thermodynamic parameters of NiTiC1 and NiTiC2 alloys. In addition, the microstructures and their relations with the determined phase transformation temperatures and thermodynamic parameters were determined for the alloys.

## 2 Experimental Procedure

Powders with 99.8% purity of nickel, titanium, and C (in at.%) to make of Ni-48.72Ti-0.4C and Ni-48.32Ti-0.8C were compressed to small pellets by a hydraulic press. They were then melted several times in an electric arc melting furnace. Before melting, all the air in the chamber was vacuumed and filled with argon gas, thus greatly reducing the likelihood of oxidation in the alloys at high temperatures during melting. The atomic ratios

(at.%) and weight ratios (wt.%) of the produced alloys are given in Table 1.

Alloy ingots were homogenized for 24 hours in a muffle furnace under argon atmosphere and 900 °C temperature, then, cooled in ice brine water to obtain the martensitic phase by minimizing the amount of some precipitates that may occur in the synthesis process of the alloys.

**Table 1.** The nominal codes for the produced alloys.

| Alloys | Compositional rate (wt.%) | | | Compositional rate (at.%) | | |
|---|---|---|---|---|---|---|
| | Ni | Ti | C | Ni | Ti | C |
| **NiTiC1** | 56.10 | 43.81 | 0.09 | 50.88 | 48.72 | 0.4 |
| **NiTiC2** | 56.25 | 43.57 | 0.18 | 50.88 | 48.32 | 0.8 |

Samples of alloys were cut from the alloys in suitable sizes to be measured by Differential Scanning Calorimeter (DSC), X-ray diffraction (XRD), Scanning Electron Microscopy (SEM), and Chemical Analysis (EDX) analyses. In order to determine the transformation temperatures by DSC, the cut samples were re-homogenized for 30 minutes to avoid shear forces formed during cutting. The DSC measurements were made at a 10 °C/min heating/cooling rate and in an $N_2$ gas environment. $A_s$ (Austenite start), $A_f$ (Austenite finish), $M_s$ (Martensite start), and $M_f$ (Martensite finish) transformation temperatures; $A_p$ (Austenite peak), $M_p$ (Martensite peak), and $T_0$ (equilibrium temperatures) temperatures; and $\Delta H$ (Enthalpy) were obtained using the DSC results. X-ray measurement was accomplished by the RIGAKU ULTIMA IV X-Ray Diffraction Spectrometer at room temperature between 30-80° and a constant scan rate of 2 °/min. To obtain the surface micrograph analysis of the alloys, the samples were ground, polished, and chemically etched using a solution containing $10HNO_3 + 25HF + 150H_2O$, then, SEM-EDX compositional analysis were carried out using the JEOL JSM 6510 electron microscope.

## 3 Results and Discussions

Figure 1 illustrates the XRD pattern of the NiTiC1 and NiTiC2 alloys. In the literature, it has been determined that $B19'$ martensite, $B2$ austenite, and $Ni_4Ti_3$ precipitation phases can be formed in NiTi alloys, while TiC phases are generally present in C doped compositions [6, 14, 22-25]. $B2$ austenite, $Ni_4Ti_3$ precipitation and, TiC phase peaks were found in NiTiC1 and NiTiC2 alloys that are compatible with the literature. $B19'$ martensite peaks were not found because the martensite phase transformations were below room temperature. However, using $B19' \rightarrow B2$ phase transformation obtained by the DSC thermo-gram, the presence of $B19'$ was determined. Among the peaks determined in the alloy, it is seen that the $B2$ austenite phase peak is more dominant than the other peaks. The fact that the $B2$ austenite phase was more dominant than the $B19'$ martensite phase was due to the XRD analysis of the alloys was found at room temperature. On the other hand, it was determined that the

peaks belonging to the $Ni_4Ti_3$ precipitation phase have low intensity. The XRD result gives more information about crystal structure and other parameters such as crystallite size ($D$) of the alloys. Scherrer's model is based on the full width at half-maximum ($FWHM$ ($B$)), the wavelength of the X-ray ($k$), and the angle ($\theta$) in radians, which can be expressed as follows [26, 27]:

$$D = K\lambda / B \cos\theta \qquad (1)$$

where $K$ is the Scherrer constant and its best approximation value is 0.9. $\lambda$ is the wavelength of the X-ray source used ($\lambda_{K\alpha}$ ($Cu$) = 1.5406 Å) and $B$ represents the Bragg angle. Crystallite size is an important parameter of the effects strength, damping capacity, latent heat, and temperature dependence of materials. It is known that the material with nanoscale crystallite sizes (<100 nm) generally contributes positively to the microstructure and mechanical behavior [28, 29]. The crystallite size of the alloys is given in Table 2. The results reveal that the crystallite size is below 100 nm.
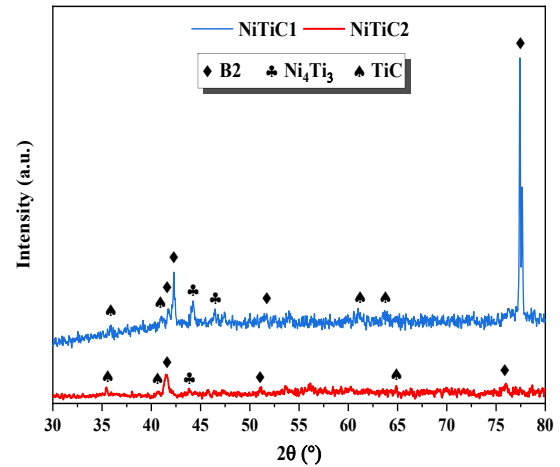


**Figure 1**. X-ray patterns of the NiTiC1 and NiTiC2 alloys.

**Table 2.** The valence electrons per atom ($e_v/a$) and valence electrons concentration ($c_v$) of the NiTiC1 and NiTiC2 alloys.

| Alloys | $e_v/a$ | $c_v$ | Crystallite size (nm) |
|---|---|---|---|
| **NiTiC1** | 7.366 | 0.291 | 88.60 |
| **NiTiC2** | 7.375 | 0.291 | 24.13 |

Figure 2 depicts the SEM micrographs of the NiTiC1 and NiTiC2 alloys taken to determine the surface structures. Since, the martensite phase transformation of the alloys is below room temperature, so the martensite plates are not clearly observed. On the other hand, the $Ni_4Ti_3$ precipitated phases in both alloys are observed in the form of pits and scattered over the entire surface. The EDX results are given in Table 3. The EDX results of NiTiC1 alloy show that there is no evidence of the presence of C element in the composition of the precipitate phases. While the precipitate phases formed in NiTiC2 alloy contains C element.
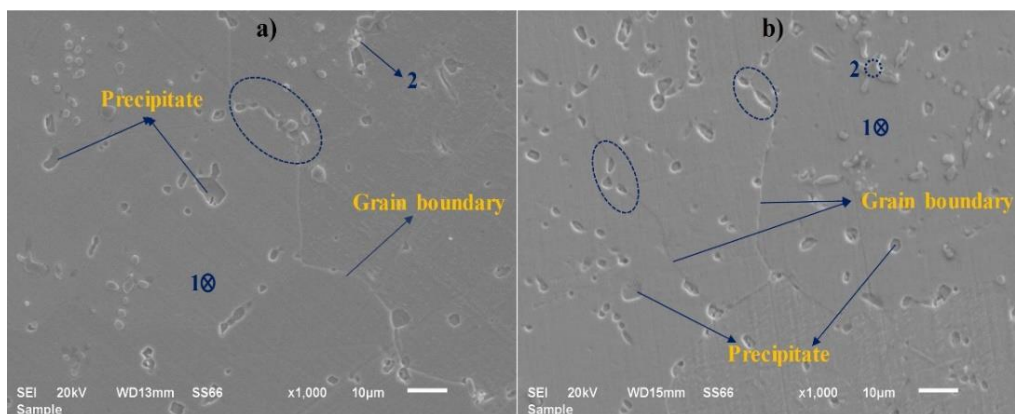
**Figure 2**. SEM micrograph of the NiTiC1 and NiTiC2 alloys.

**Table 3.** Chemical composition results for determined areas on the SEM images of NiTiC1 and NiTiC2 alloys.

| Alloys | Location | Ni (at.%) | Ti (at.%) | C (at.%) |
|--------|----------|-----------|-----------|----------|
| **NiTiC1** | **Precipitate** | 43.83 | 56.17 | 0.0 |
| | 1 | 49.78 | 50.22 | 0.0 |
| | 2 | 39.95 | 52.34 | 7.71 |
| **NiTiC2** | **Precipitate** | 39.17 | 57.36 | 3.47 |
| | 1 | 46.81 | 46.63 | 6.56 |
| | 2 | 32.26 | 49.76 | 17.98 |

The EDX analysis results obtained from dark areas (region no. 1) showed that the Ti concentration is higher than the Ni concentration. It is noteworthy that the regions with a high Ti ratio are matrix phase has a flat and uni-color appearance. The bright structures (no. 2) observed on the surfaces of both alloys are different from the precipitates and region no. 1. Therefore, it is noticed that C elements are concentrated in the bright regions in both alloys, which is believed to be C rich Ti compound, possibly TiC. Since, the electron beam size for the EDX analysis a few microns, it is possible to indicate that signals from matrix phase is also plentiful and reduce the concentration of C in such regions. At high temperatures, Ti is more likely to bond with C compared to Ni because it needs lower activation energy. Another structure determined from SEM images is grain boundaries. The grains found in SEM images are different from the crystallites obtained through XRD analysis and through the mathematical equation. It is observed that the grain boundaries determined in both alloys were interrupted due to the compact precipitations formed along the boundaries.

The transformation temperatures ($A_s$, $A_f$) during heating and ($M_s$, $M_f$) during cooling; the $\Delta H^{A \leftrightarrow M}$ energies of the martensitic phase transformations for the carbon-added Nickel-rich NiTi alloys showed in Figure 3. In general, it is known that the end product of martensite transformations of NiTi alloys has $B19'$ (monoclinic) crystal structure, while the main phase has $B2$ (cubic) crystal structure [4]. NiTiC1 and NiTiC2 alloys showed a one-step phase transformation from martensite to austenite (during the endothermic process) and from austenite to martensite (through the exothermic process) in the heating/cooling curves, i.e., phase transformation occurred as $B19' \rightarrow B2$, during heating, and as $B2 \rightarrow$

$B19'$ during cooling. The low volume fraction of $Ni_4Ti_3$ precipitates forming the $R$ (Rhombohedral) phase caused no transformation of the $R$ phase in the alloys [14]. The austenite and martensite phase transformation temperatures during the transformation are given in Table 4.
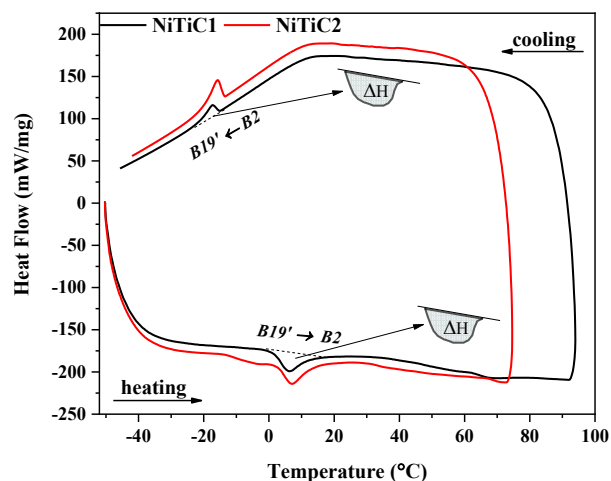


**Figure 3**. DSC curves of the NiTiC1 and NiTiC2 alloys at 10 ºC/min heating/cooling rates.

**Table 4.** Transformation temperatures of the NiTiC1 and NiTiC2 alloys.

| Alloys | $A_s$ (°C) | $A_p$ (°C) | $A_f$ (°C) | $M_s$ (°C) | $M_p$ (°C) | $M_f$ (°C) | $H_t$ (°C) |
|--------|------|------|------|------|------|------|------|
| **NiTiC1** | 2.9 | 6.6 | 11.7 | -14.3 | -15.4 | -20.0 | 26.0 |
| **NiTiC2** | 2.2 | 5.7 | 11.7 | -15.4 | -16.9 | -18.4 | 27.1 |

When Figure 3 and Table 4 were examined, it was found that the transformation temperatures of the alloys were below room temperature (25°C). The transformation and hysteresis temperatures of the alloys changed with changing the amount of C. It is known from previous studies that changes in hysteresis temperature are caused by internal frictions (dispersion energy) in the microstructure [7]. In addition, it was concluded that the increase in C atom ratios expanded the hysteresis temperature and thus slowed down the phase transformation process.

One of the parameters that change the precipitation of $Ni_4Ti_3$ in the matrix is the concentration of the elements. Only a small amount of $Ni_4Ti_3$ precipitate phases were found in the SEM-EDX of NiTiC1 and NiTiC2 alloys, resulting from the C addition into the nitinol. Thus, the

presence of $R$ phase caused by $Ni_4Ti_3$ precipitated phases was not detected in DSC analysis. It was determined that this change in the matrix caused the $Ni_4Ti_3$ precipitation phases to be located between the grain boundaries as a result of the absence of the $R$ phase.

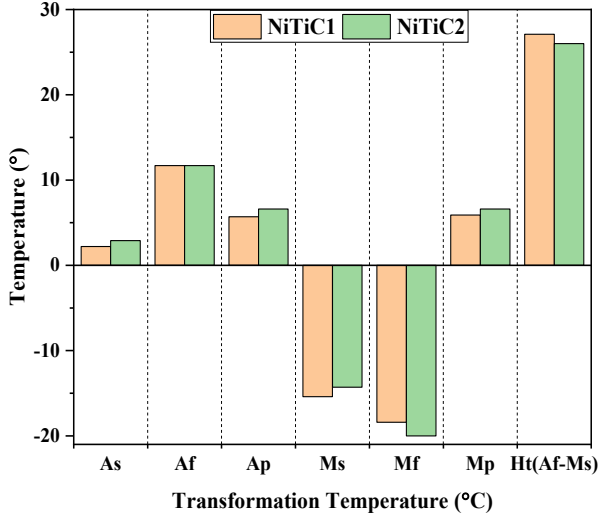Figure 4 reveals the variation of the transformation and hysteresis temperature of the alloys.



**Figure 4**. Variation of transformation and hysteresis temperatures of NiTiC1 and NiTiC2 alloys.

$A_f$ and $M_s$ phase transformation temperatures were used to calculate equilibrium temperature ($T_0$) by equation (2), and entropy change ($\Delta S^{A\to M}$ and $\Delta S^{M\to A}$) for austenite and martensite phase transformation were calculated using equation (3) [15, 32];

$$T_0 = 1/2 \left(A_f + M_s\right), \tag{2}$$
$$\Delta S^{A\leftrightarrow M} = \Delta H^{A\leftrightarrow M}/T_0 . \tag{3}$$

The equilibrium temperature is where the Gibbs free energies of reverse phase transformation and $\Delta G^{A\to M}(T_0)$ is zero, such that [15];

$$\begin{aligned}\Delta G^{A\to M}(T_0) &= G^M(T_0) - G^A(T_0) \\ &= (H^M - T_0 S^M) - (H^A - T_0 S^A) \\ &= \Delta H^{A\to M} - T_0 \Delta S^{A\to M} = 0\end{aligned} \tag{4}$$

where $G^{M,A}$, $S^{M,A}$, and $H^{M,A}$ are the Gibbs free energy, entropy, and enthalpy of the martensite phase.

The free energy difference is called the driving force required for phase transformation. The driving force is reason for a reaction like the diffusion in a solution, which generally causes a grain growth or a phase transformation, resulting from the change in temperature or chemical in-homogeneity [31]. The Gibbs free energy at the initial martensite temperature ($M_s$) can be calculated by using the following equation [33];

$$\begin{aligned}\Delta G^{A\to M}(M_s) &= \Delta G^{M\to A}(T_0) - \Delta G^{M\to A}(M_s) \\ &= -(T_0 - M_s S^M)\Delta S^{M\to A}\end{aligned} \tag{5}$$

Elastic energy stored or released during transformation will inhibit the forward transformation but will aid the reverse transformation. The difference between the reverse transformation temperatures ($M_s$ and $M_f$) is proportional to the amount of elastic energy stored. The value of elastic energy was found by [34];

$$\begin{aligned}G_e &= \Delta G^{M\to A}(M_s) - \Delta G^{M\to A}(M_f) \\ &= (M_s - M_f)\Delta S^{M\to A}\end{aligned} \tag{6}$$

$T_0$, $\Delta S^{A\leftrightarrow M}$, $\Delta G^{M\to A}$ and $G_e$ values were calculated by Equation (2-5, 6) and the results are listed in Table 5. The energies of the alloy $\Delta H^{A\to M}$ (austenite to martensite) and $\Delta H^{M\to A}$ (martensite to austenite) are one of the important thermodynamic parameters in alloys exhibiting martensitic transformation. The energy values of $\Delta H^{A\to M}$ and $\Delta H^{M\to A}$ of C-reinforced NiTiC1 and NiTiC2 alloys are given in Table 5.

**Table 5.** Some thermodynamic parameters of NiTiC1 and NiTiC2 alloys.

| Alloys | $T_0$ (°C) | $\Delta G^{A\leftrightarrow M}$ (J) | $G_e$ (J) | $\Delta S^{A\to M}$ (J/kg°C) | $\Delta S^{M\to A}$ (J/kg°C) | $\Delta H^{A\to M}$ (J/g) | $\Delta H^{M\to A}$ (J/g) |
|---|---|---|---|---|---|---|---|
| NiTiC1 | 13.0 | 96 | 412 | 72.3 | 73.8 | 0.94 | 0.96 |
| NiTiC2 | 13.4 | 133 | 115 | 35.1 | 78.3 | 0.47 | 1.05 |

Among NiTiC1 and NiTiC2 alloys, whose thermodynamic parameters are given in Table 5, the most striking parameter is the elastic energy. It is seen that the elastic energy decreases approximately three times with the increase of C reinforcement. It means that it contributes more to the reverse transformation that occurs in NiTiC1 alloy compared to NiTiC2, owing to the high elastic energy stored in NiTiC1 alloy during the reverse transformation. In addition, it is concluded that the larger crystallite size of NiTiC1 alloy than that of NiTiC2 contributes to the high amount of elastic energy stored in NiTiC1 alloy.

## 4 Conclusion

The transformation temperatures and some thermodynamic parameters of NiTiC1 and NiTiC2 SMAs produced by the arc-melting method were investigated by the DSC analysis system. Their microstructures were examined by XRD and SEM-EDX analysis. As a result of the analysis, the following findings were drawn;

- The transformation temperatures of the alloys were found to be below the room temperature. The transformation exhibited a one-step phase transformation and was observed to be $B19' \to B2$ during heating and as $B2 \to B19'$ during cooling. By increasing the C concentration, the transformation temperatures varied between 0.7 and 1.5 °C.

- As the C concentration increase, internal friction, and dislocations of the alloy increase during the martensite transformation resulting in the value of temperature hysteresis $sH_t$, and Gibbs Free energies ($\Delta G^{A \rightarrow M}$) decreased.
- It was determined that martensite plates and martensite peaks were not observed in SEM-EDX and XRD analyses carried out at room temperature. $B2$ austenite, $Ni_4Ti_3$ precipitation, and TiC phases were determined by XRD analysis. The existence of these phases was supported by SEM-EDX analysis, too.
- It was determined that the grain boundaries were formed along with the $Ni_4Ti_3$ precipitation phases. The crystallite size of the alloys was calculated to be less than 100 nm.

## Acknowledgments

## References

[1] Otsuka, K., & Ren, X. (2005). Physical metallurgy of Ti–Ni-based shape memory alloys. *Progress in materials science*, 50(5), 511-678.

[2] Jani, J. M., Leary, M., Subic, A., & Gibson, M. A. (2014). A review of shape memory alloy research, applications and opportunities. *Materials & Design* (1980-2015), 56, 1078-1113.

[3] Balci, E., & Dağdelen, F. (2021). Investigate of Microhardness and Microstructure of Ti-Ni-Nb-X (Ta and V) Shape Memory Alloys. *International Journal of Innovative Engineering Applications*, 5(2), 131-135.

[4] Dagdelen, F., & Ercan, E. (2014). The surface oxidation behavior of Ni–45.16% Ti shape memory alloys at different temperatures. *Journal of Thermal Analysis and Calorimetry*, 115(1), 561-565.

[5] Kök, M., Al-Jaf, A. O. A., Çirak, Z. D., Qader, I. N., & Özen, E. (2020). Effects of heat treatment temperatures on phase transformation, thermodynamical parameters, crystal microstructure, and electrical resistivity of NiTiV shape memory alloy. *Journal of Thermal Analysis and Calorimetry*, 139(6), 3405-3413.

[6] Kaya, I., Karaca, H., Nagasako, M., Kainuma, R., Effects of aging temperature and aging time on the mechanism of martensitic transformation in nickel-rich NiTi shape memory alloys, *Materials Characterization,* 159, 110034, 2020.

[7] Kaya, I., Karaca, H. E., Nagasako, M., & Kainuma, R. (2020). Effects of aging temperature and aging time on the mechanism of martensitic transformation in nickel-rich NiTi shape memory alloys. *Materials Characterization*, 159, 110034.

[8] Eskil, M. (2013). The effect of aging temperature on transformation parameters of porous NiTi shape memory alloy fabricated by SHS. *Russian Journal of Non-Ferrous Metals*, 54(1), 104-111.

[9] Dal, S., Demirel, B., & Eskil, M. (2021). The effects of homogenization time on the crystal structure and hardness of NiMnGaMo alloy. *Engineering Science and Technology, an International Journal*, 24(2), 493-502.

[10] Siddharth, M. K., & Sarada, B. N. (2021). Effect of heat treatment time and temperature variants on Ni-Ti shape memory alloy. *Materials Today: Proceedings*.

[11] Naji, H., Khalil-Allafi, J., & Khalili, V. (2020). Microstructural characterization and quantitative phase analysis of Ni-rich NiTi after stress assisted aging for long times using the Rietveld method. *Materials Chemistry and Physics*, 241, 122317.

[12] Ryklina, E. P., Polyakova, K. A., & Prokoshkin, S. D. (2021). Role of Nickel Content in One-Way and Two-Way Shape Recovery in Binary Ti-Ni Alloys. *Metals*, 11(1), 119.

[13] Belyaev, S., Resnina, N., Iaparova, E., Ivanova, A., Rakhimov, T., & Andreev, V. (2019). Influence of chemical composition of NiTi alloy on the martensite stabilization effect. *Journal of Alloys and Compounds*, 787, 1365-1371.

[14] Qin, Q., Peng, H., Fan, Q., Zhang, L., & Wen, Y. (2018). Effect of second phase precipitation on martensitic transformation and hardness in highly Ni-rich NiTi alloys. *Journal of Alloys and Compounds,* 739, 873-881.

[15] Frenzel, J., Zhang, Z., Somsen, C., Neuking, K., & Eggeler, G. (2007). Influence of carbon on martensitic phase transformations in NiTi shape memory alloys. *Acta Materialia*, 55(4), 1331-1341.

[16] Goryczka, T. (2008). Martensitic transformation in Ni–Ti–Co strip produced by twin roll casting. *Materials Science and Engineering*: A, 481, 676-679.

[17] Tong, Y. X., Liu, J. T., Feng, C. H. E. N., Liang, C. Q., Bing, T. I. A. N., Li, L. I., & Zheng, Y. F. (2014). Effect of aging on martensitic transformation and superelasticity of TiNiCr shape memory alloy. *Transactions of Nonferrous Metals Society of China*, 24(8), 2598-2605.

[18] Basu, R., Eskandari, M., Upadhayay, L., Mohtadi-Bonab, M. A., & Szpunar, J. A. (2015). A systematic investigation on the role of microstructure on phase transformation behavior in Ni–Ti–Fe shape memory alloys. *Journal of Alloys and Compounds,* 645, 213-222.

[19] Wang, M., Jiang, M., Liao, G., Guo, S., & Zhao, X. (2012). Martensitic transformation involved mechanical behaviors and wide hysteresis of NiTiNb shape memory alloys. *Progress in natural science: materials international*, 22(2), 130-138.

[20] Ramaiah, K. V., Saikrishna, C. N., & Bhaumik, S. K. (2014). Ni24. 7Ti50. 3Pd25. 0 high temperature shape memory alloy with narrow thermal hysteresis and high thermal stability. *Materials & Design* (1980-2015), 56, 78-83.

[21] Fraj, B. B., Zghal, S., & Tourki, Z. (2017, March). DSC investigation on entropy and enthalpy changes in Ni-rich NiTi shape memory alloy at various cooling/heating rates. In *International Conference Design and Modeling of Mechanical Systems* (pp. 631-639). Springer, Cham.

[22] Wang, J., Pan, Z., Wang, Y., Wang, L., Su, L., Cuiuri, D., ... & Li, H. (2020). Evolution of crystallographic orientation, precipitation, phase transformation and mechanical properties realized by enhancing deposition current for dual-wire arc additive manufactured Ni-rich NiTi alloy. *Additive Manufacturing*, 34, 101240.

[23] Pandolfi, G. S., Martins, S. C., Buono, V. T., & Santos, L. A. (2020). Precipitation kinetics of Ti3Ni4 and multistage martensitic transformation in an aged Ni–rich Ni–Ti shape memory alloy. *Journal of Materials Research and Technology,* 9(4), 9162-9173.

[24] Chen, F., Tong, Y. X., Lu, X. L., Wang, X., Tian, B., Li, L., ... & Ma, L. W. (2011). Effect of graphite addition on martensitic transformation and damping behavior of NiTi shape memory alloy. *Materials Letters*, 65(7), 1073-1075.

[25] Vallauri, D., Adrián, I. A., & Chrysanthou, A. (2008). TiC–TiB2 composites: A review of phase relationships, processing and properties. *Journal of the European Ceramic Society, 28(8)*, 1697-1713.

[26] Qader, I. N., Kok, M., & Cirak, Z. D. (2021). The effects of substituting Sn for Ni on the thermal and some other characteristics of NiTiSn shape memory alloys. Journal of *Thermal Analysis and Calorimetry,* 145(2), 279-288.

[27] Tankut, A. T. E. Ş., KÖYTEPE, S., BULUT, N., & KAYGİLİ, O. Ni Katkısının Fe2O3'ün Yapısal Özellikleri Üzerine Etkilerinin Araştırılması. *International Journal of Innovative Engineering Applications*, 5(2), 81-87.

[28] Chen, J., Yin, H., & Sun, Q. (2020). Effects of grain size on fatigue crack growth behaviors of nanocrystalline superelastic NiTi shape memory alloys. *Acta Materialia*, 195, 141-150.

[29] Shi, X., Cui, L., Jiang, D., Yu, C., Guo, F., Yu, M., ... & Liu, Y. (2014). Grain size effect on the R-phase transformation of nanocrystalline NiTi shape memory alloys. *Journal of Materials Science*, 49(13), 4643-4647.

[30] Mohammed, S. S., Kok, M., Qader, I. N., Kanca, M. S., Ercan, E., Dağdelen, F., & Aydoğdu, Y. (2020). Influence of Ta additive into Cu84− xAl13Ni3 (wt%) shape memory alloy produced by induction melting. *Iranian Journal of Science and Technology, Transactions A: Science*, 44(4), 1167-1175.

[31] Callister, W. D., & Rethwisch, D. G. (2018). *Materials science and engineering: an introduction* (Vol. 9). New York: Wiley.

[32] Ercan, E., Dagdelen, F., & Qader, I. N. (2020). Effect of tantalum contents on transformation temperatures, thermal behaviors and microstructure of CuAlTa HTSMAs. *Journal of Thermal Analysis and Calorimetry*, 139(1), 29-36.

[33] Dagdelen, F., Balci, E., Qader, I., Ozen, E., Kok, M., Kanca, M., & Mohammed, S. (2020). Influence of the Nb content on the microstructure and phase transformation properties of NiTiNb shape memory alloys, *JOM,* 72(4), 1664-1672.

[34] Dagdelen, F., Kok, M., & Qader, I. N. (2019). Effects of Ta content on thermodynamic properties and transformation temperatures of shape memory NiTi alloy. *Metals and Materials International,* 25(6), 1420-1427.